# A Low-Toxic Multifunctional Nanoplatform Based on $Cu_9S_5$@$mSiO_2$ Core-Shell Nanocomposites: Combining Photothermal- and Chemotherapies with Infrared Thermal Imaging for Cancer Treatment

*Guosheng Song, Qian Wang, Yang Wang, Gang Lv, Chun Li, Rujia Zou, Zhigang Chen, Zongyi Qin, Keke Huo, Ronggui Hu, and Junqing Hu**

**Copper chalcogenides have been demonstrated to be a promising photothermal agent due to their high photothermal conversion efficiency, synthetic simplicity, and low cost. However, the hydrophobic and less biocompatible characteristics associated with their synthetic processes hamper widely biological applications. An alternative strategy for improving hydrophilicity and biocompatibility is to coat the copper chalcogenide nanomaterials with silica shell. Herein, the rational preparation design results in successful coating mesoporous silica ($mSiO_2$) on as-synthesized $Cu_9S_5$ nanocrystals, forming $Cu_9S_5$@$mSiO_2$-PEG core-shell nanostructures. As-prepared $Cu_9S_5$@$mSiO_2$-PEG core-shell nanostructures show low cytotoxicity and excellent blood compatibility, and are effectively employed for photothermal ablation of cancer cells and infrared thermal imaging. Moreover, anticancer drug of doxorubicin (DOX)-loaded $Cu_9S_5$@$mSiO_2$-PEG core-shell nanostructures show pH sensitive release profile and are therefore beneficial to delivery of DOX into cancer cells for chemotherapy. Importantly, the combination of photothermal- and chemotherapies demonstrates better effects of therapy on cancer treatment than individual therapy approaches in vitro and in vivo.**

## 1. Introduction

Photothermal therapy (PTT), as a minimally invasive therapeutic methodology, employs hyperthermia generated by photothermal agents from laser energy to kill cancer cells.[1] Such a PPT prefers near-infrared (NIR, $\lambda$ = 700–1100 nm) radiation with the typical tissue penetration of several centimeters in biological tissues[2] and has attracted much attention in recent years as a promising alternative or supplement to traditional cancer therapies. Currently, several kinds of nanomaterials with strong light absorbing capability have shown the encouraging photothermal therapeutic effects in vitro and in vivo experiments. Metal nanostructures are the most widely explored class of the PTT agents, including Au and Pd nanomaterials (such as Au nanoparticles,[3] Au nanorods,[4] Au nanocages,[5] Au nanoshells,[6] and Pd nanosheets[7]), due to their tunable surface plasmon resonance (SPR) properties. However, their practical applications are limited by the high cost of noble-metal based materials.[1c] Also, carbon nanomaterials (including carbon nanotubes[8] and graphene[9]) and some organic compounds such as conductive nanoparticles (e.g., PEDOT:PSS,[1b] polypyrrole,[10] and polyaniline[11]) have shown effective PTT to cancer. Recently, copper chalcogenides have proven to be a promising candidate as a photothermal agent due to their low cost and high photothermal conversion efficiency as well as synthetic simplicity.[1c,2b,12] Our previous works have demonstrated that the CuS flower-like superstructures[2b] and $Cu_9S_5$

G. Song, C. Li, Dr. R. Zou, Prof. Z. Chen,
Prof. Z. Qin, Prof. J. Hu
State Key Laboratory for Modification of Chemical Fibers
and Polymer Materials
College of Materials Science and Engineering
Donghua University
Shanghai 201620, China
E-mail: hu.junqing@dhu.edu.cn
Dr. Q. Wang
Department of Orthopaedics
Shanghai First People's Hospital
Shanghai Jiaotong University
100 Haining Road, Hongkou District, Shanghai 200080, China

Y. Wang, Prof. K. Huo
State Key Laboratory of Genetic Engineering
School of Life Sciences
Fudan University
Shanghai 200433, China
G. Lv
The First Department of Comprehensive Treatment
Eastern Hepatobiliary Surgery Hospital
Second Military Medical University
Shanghai 200438, China
Prof. R. Hu
State Key Laboratory of Molecular Biology
Institute Biochemistry & Cell Biology
Shanghai Institutes for Biological Sciences
Chinese Academy of Sciences
Shanghai 200031, China

DOI: 10.1002/adfm.201203317

nanoplates[1c] are efficient 980-nm laser-driven photothermal agents and can effectively kill cancer cells in vitro and in vivo. As we know, the PPT agents as a platform for therapy applications should fulfill the following requirements: strong absorbance in NIR region and efficient conversion of the laser energy into heat, and high biocompatibility for a successful applications in vivo therapy.[13] Thus, it is necessary that the copper chalcogenides should possess good hydrophilicity and low toxicity in a biological environment. However, as-prepared copper chalcogenides are hydrophobic and thus less biocompatible when synthesized via thermal decomposition.[1c,12b] Though several surface modification methods such as ligands exchange[1c] or polymer coating[12b] have been adopted to make these copper chalcogenides hydrophilic properties, they still show a considerable toxicity in vitro,[1c] thus limiting their wide applications in vivo therapy. Therefore, new methodologies of surface modification are still developed to further reduce the toxicity of the copper chalcogenides as PTT agents.

An alternative strategy for reducing the toxicity is to coat the copper chalcogenide nanomaterials with a silica shell, as this shell can protect the nanomaterials from the external environment and thereby improve the stability and biocompatibility.[14] In particular, if mesoporous silica ($mSiO_2$) as a biocompatible shell is coated on the copper chalcogenide nanomaterials, it will result in the copper chalcogenide@$mSiO_2$ core-shell nanostructures. Within such core-shell nanostructures, the core of copper chalcogenides can effectively convert NIR laser into heat for ablation of cancer cells and infrared thermal imaging, meanwhile, the shell of $mSiO_2$ is much easier to incorporate guest molecules (such as anticancer drug[4d,15] or therapeutic oligonucleotides[16]) into the mesoporous channels for chemo- or gene-therapy and to further bioconjugate with functional groups (folate,[17] peptide,[16a,18] and DNA[19]) on the outermost surface for targeting delivery to tumor.[19a] Therefore, it is expected that the copper chalcogenide@$mSiO_2$ core-shell nanostructures not only possess high biocompatibility, but also are a potential multifunctional platform for effective photothermal and chemotherapy and infrared thermal imagining applications.

Herein, we report the rational design and successful synthesis of the $Cu_9S_5$@$mSiO_2$-PEG core-shell nanostructures by a thermal decomposition reaction and a sol-gel reaction, followed by surface modification. As-prepared $Cu_9S_5$@$mSiO_2$-PEG core-shell nanostructures show a low cytotoxicity and excellent blood compatibility in vitro, and can also be effective photothermal ablation of cancer cells and infrared thermal imaging. Moreover, anticancer drug of doxorubicin (DOX) -loaded $Cu_9S_5$@$mSiO_2$-PEG core-shell nanostructures can effectively delivery DOX into cancer cells with pH sensitive release profile and be employed for chemotherapy of cancer cells. Importantly, the combination of photothermal- and chemotherapies demonstrates better therapy effects on cancer cells than individual therapy approaches in vitro and in vivo.

## 2. Results and Discussion

The $Cu_9S_5$@$mSiO_2$-PEG core-shell nanostructures were synthesized by combining a modified thermal decomposition reaction and a sol-gel reaction, followed by surface modification. **Figure 1**a illustrates the synthetic procedure of the $Cu_9S_5$@$mSiO_2$-PEG core-shell nanocomposites. First, hydrophobic $Cu_9S_5$ nanocrystals were transferred into an aqueous phase by utilizing cetyltrimethylammonium bromide (CTAB). Subsequently, CTAB-stabilized $Cu_9S_5$ nanocrystals ($Cu_9S_5$/CTAB) were coated with mesoporous silica shells through hydrolysis and condensation of tetraethylorthosilicate (TEOS) processes, forming $Cu_9S_5$@$mSiO_2$ core-shell composite nanoparticles. As-obtained $Cu_9S_5$@$mSiO_2$ core-shell nanoparticles were then

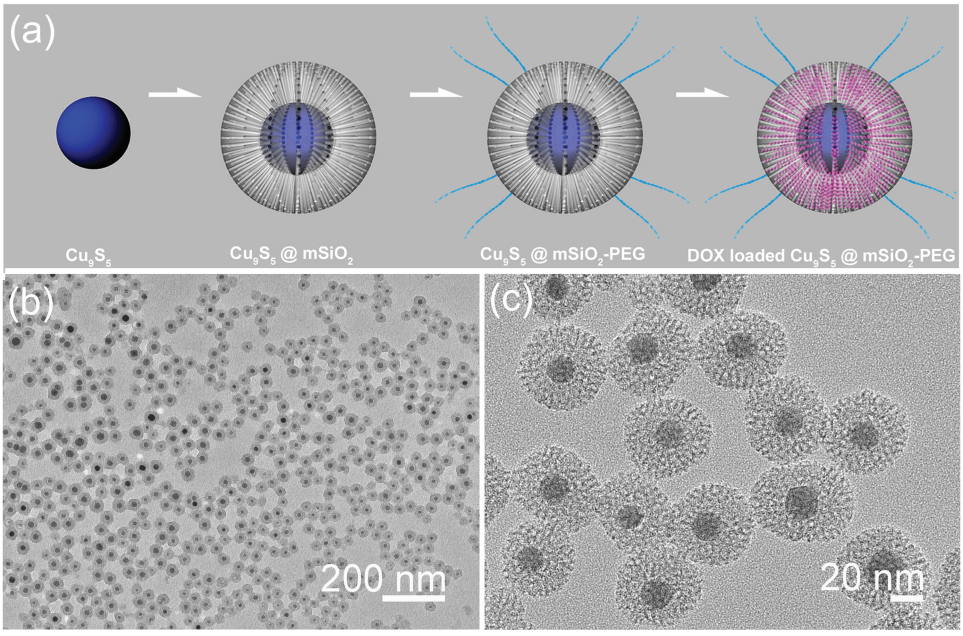


**Figure 1.** a) Schematic illustration of the synthetic protocol of the $Cu_9S_5$@$mSiO_2$-PEG core-shell nanocomposites. b,c) Low- and high- magnification TEM images of as-synthesized $Cu_9S_5$@$mSiO_2$-PEG core-shell nanocomposites, respectively.

modified by poly(ethylene glycol)-silane (PEG-silane) on their outmost surfaces, forming $Cu_9S_5$@$mSiO_2$-PEG core-shell nanocomposites, which were further hydrothermally treated to enhance the stability of the mesoporous silica shells.[20] The CTAB template was then removed via an ion exchange method before bioapplications. Lastly, anticancer drug of doxorubicin (DOX) was loaded in the $Cu_9S_5$@$mSiO_2$-PEG core-shell nanocomposites for later photothermal- and chemotherapy applications.

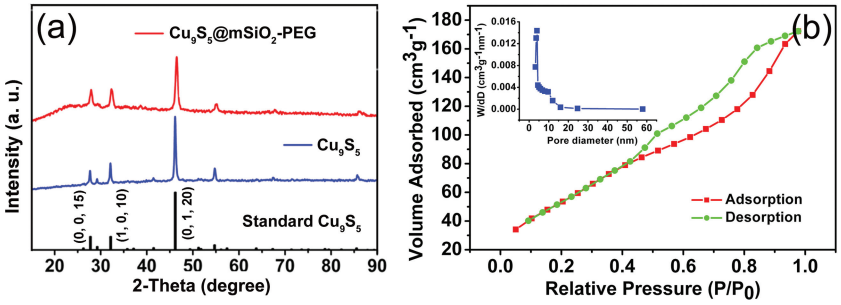


**Figure 2.** a) XRD patterns of the synthesized $Cu_9S_5$ nanocrystals and $Cu_9S_5$@$mSiO_2$-PEG core-shell nanocomposites, as referenced by standard $Cu_9S_5$ phase. b) $N_2$ adsorption/desorption isotherms and corresponding pore-size distribution curve (inset) of the $Cu_9S_5$@$mSiO_2$-PEG core-shell nanocomposites.

Supporting Information Figure S1a shows a representative transmission electron microscopy (TEM) image of as-obtained oleylamine-capped $Cu_9S_5$ nanocrystals. As depicted, the oleylamine-capped $Cu_9S_5$ nanocrystals have a well-defined morphology with an average diameter of ~20 nm and high crystallinity, as evidenced by high resolution TEM (HRTEM) image (Supporting Information Figure S1b). Prior to the mesoporous $SiO_2$ coating, the oleylamine-capped $Cu_9S_5$ nanocrystals have been modified by the CTAB in order to endow their hydrophilic property and facilitate the $SiO_2$ coating, the resulting size and crystallinity of which remained unchanged, suggested by the TEM and HRTEM imaging (Supporting Information Figure S1c,d). After being coated with the $SiO_2$ shells, the $Cu_9S_5$@$mSiO_2$ core-shell nanoparticles were modified by PEG on their outmost surfaces, followed by hydrothermal treatment and removal of the CTAB. Figure 1b shows the typical TEM image of the final $Cu_9S_5$@$mSiO_2$-PEG core-shell nanocomposites with a uniform diameter of ≈45 nm, in which one $Cu_9S_5$ core is encapsulated into one $mSiO_2$ shell, appearing like many frog eggs. The mesoporous characteristic of the silica shells is evidently exhibited by a high-magnification TEM image (Figure 1c), which will offer an opportunity for a general drug carrier. Supporting Information Figure S1f shows the HRTEM image of the $Cu_9S_5$@$mSiO_2$-PEG core-shell nanocomposites, in which the clearly resolved crystal lattice demonstrates a defined crystal structure of the $Cu_9S_5$ core material.

**Figure 2**a reveals X-ray powder diffraction (XRD) patterns of the as-prepared $Cu_9S_5$ nanocrystals and $Cu_9S_5$@$mSiO_2$-PEG core-shell nanocomposites. Several well-defined characteristic peaks such as (0, 0, 15), (1, 0, 10) and (0, 1, 20) exhibit the rhombohedral $Cu_9S_5$ phase, referenced by standard $Cu_9S_5$ phase (JCPDS card no: 47-1748). While in the $Cu_9S_5$@$mSiO_2$-PEG core-shell nanocomposites, a wide and weak peak at $2\theta \approx 23°$ is clearly due to amorphous silica coating[21]within such composites. The $N_2$ adsorption-desorption isotherms, Figure 2b, show a characteristic type IV isotherm,[22] demonstrating their mesoporous structure characteristics. The average pore diameter was calculated to be 4 nm with a narrow size distribution from the adsorption branch of the isotherm by using the Barrett-Joyner-Halenda (BJH) model. Brunauer-Emmett-Teller (BET) surface area and BJH pore volume are calculated to be as large as 221 $m^2\ g^{-1}$ and 0.224 $cm^3\ g^{-1}$, respectively, which will guarantee a high drug payload.

The oleylamine-capped $Cu_9S_5$ nanocrystals are hydrophobic (Supporting Information Figure S1e, left reagent glass) and transferred into an aqueous phase (Supporting Information Figure S1e, middle reagent glass) by utilizing cetyltrimethylammonium bromide (CTAB) according to the previously reported protocols.[14e,23] Due to adsorption of the cationic surfactant (CTAB), the CTAB-stabilized $Cu_9S_5$ nanocrystals possessed a positive zeta potential (+43.2 mV, Supporting Information Figure S2a) in aqueous solution, which is facilitated for the mesoporous silica coating. Anionic silicate species from the hydrolysis of tetraethyl orthosilicate (TEOS) are deposited on the cationic CTAB soft template through an electrostatic interaction[24] and then condensate to form the mesoporous silica layer. Notably, the CTAB used as a template is hazardous and less biocompatible[25] and should be removed before bioapplications. The removal of CTAB template was carried out via a widely used method of ion exchange.[14e,15a,26] By this fast and efficient ion exchange processes, the zeta potential of the $Cu_9S_5$@$mSiO_2$ core-shell nanoparticles changed from positive charge to negative charge (–21.98 mV, Supporting Information Figure S2d), indicating the cationic CTAB was gradually removed from the mesoporous silica shells.

PEG modification of the mesoporous silica shells can significantly improve colloidal stability[20] and can effectively eliminate hemolysis induced by silica nanoparticle[27] via the formation of a biocompatible layer. Therefore, the $Cu_9S_5$@$mSiO_2$ core-shell nanoparticles were grafted with [methoxy(polyethyleneoxy) propyl]-trimethoxysilane (PEG-silane) on their outmost surfaces via covalent bonding,[14e,26] forming the $Cu_9S_5$@$mSiO_2$-PEG core-shell nanocomposites. After removal of the CTAB template, the zeta potential of the $Cu_9S_5$@$mSiO_2$-PEG core-shell nanocomposites were still negative (–22.02 mV, Supporting Information Figure S2e), which remained practically unchanged compared with that of the $Cu_9S_5$@$mSiO_2$ core-shell nanoparticles.[28] Due to the silica coating and PEG modifying the surface of the $Cu_9S_5$ nanocrystals, the $Cu_9S_5$@$mSiO_2$-PEG core-shell nanocomposites can easily be dispersed into water (**Figure S1**e, right reagent glass).

To demonstrate the successful PEG modification, the thermal gravimetric analysis (TGA) of the $Cu_9S_5$@$mSiO_2$ and $Cu_9S_5$@$mSiO_2$-PEG core-shell nanocomposites have been performed after removal of CTAB and the results are shown in Supporting Information Figure S3. The $Cu_9S_5$@$mSiO_2$ core-shell nanoparticles (red curve in Supporting Information Figure S3) show ≈7.6% of weight loss of from 250 °C to 600 °C. After PEG modification, the $Cu_9S_5$@$mSiO_2$-PEG core-shell nanocomposites display ≈13% of weight loss (black curve in Supporting

Information Figure S3). Approximately 5.4% of further weight loss at 600 °C can be attributed to the PEG decomposition, demonstrating that PEG is successfully grafted on the mesoporous silica surface.[14e] In addition, compared with the Fourier transform infrared (FTIR) spectrum of the $Cu_9S_5$@$mSiO_2$ core-shell nanoparticles (Supporting Information Figure S4, red curve), the FTIR spectrum of the $Cu_9S_5$@$mSiO_2$-PEG core-shell nanocomposites (Supporting Information Figure S4, blue curve) exhibits stronger absorption band at 2960–2855cm$^{-1}$ and absorption peaks at 1456 cm$^{-1}$ and 1350 cm$^{-1}$, which were assigned to stretching vibration of C-H,[28,29] deformation vibration of C-H[30] and the backbone of PEG,[30] respectively. Besides, the $Cu_9S_5$@$mSiO_2$-PEG core-shell nanocomposites show much enhanced colloidal stability, as compared with the $Cu_9S_5$@$mSiO_2$ core-shell nanocomposites. There is no any visible sedimentation of the $Cu_9S_5$@$mSiO_2$-PEG core-shell nanocomposites in deionized water and negligible absorption reduction in the NIR region even after 7 days, as displayed in Supporting Information Figure S5. In contrast, the $Cu_9S_5$@$mSiO_2$ core-shell nanoparticles were shown to aggregate and sediment out of the solution and their absorbance of supernatant solution in the NIR region was reduced gradually to zero after 2 days, Supporting Information Figure S5.

The optical property of the aqueous dispersion containing the $Cu_9S_5$@$mSiO_2$-PEG core-shell nanocomposites with a various concentration of $Cu^{2+}$ (i.e., 3.125, 6.25, 12.5, 25, 50 and 80 ppm) was examined by using UV-vis-NIR spectroscopy, as shown in **Figure 3**a. The concentration of $Cu^{2+}$ was determined by inductively coupled plasma atomic emission spectroscopy (ICP-AES). The spectra exhibit a minimum absorption of around 580 nm and show an increased absorption with the increase of wavelength in the NIR region ($\lambda$ = 600–1000 nm), which is due to the localized surface plasma resonances of vacancy-doped $Cu_9S_5$ core.[31] Moreover, the absorptions at 980 nm were lineally enhanced with the increase of the concentration (Figure 3b). Such a strong absorption of as-synthesized $Cu_9S_5$@$mSiO_2$-PEG core-shell nanocomposites in NIR region means a potential for their photothermal conversion upon a 980 nm laser irradiation. The photothermal conversion performance of the aqueous dispersion of the $Cu_9S_5$@$mSiO_2$-PEG core-shell nanocomposites with different concentrations was examined using the irradiation of 980 nm laser with a power density of 0.72 W/cm$^2$, as shown in Figure 3c. It is found that 80 ppm of aqueous dispersion can be heated by up to 21.3 °C in the period of 300 s, demonstrating that the $Cu_9S_5$@$mSiO_2$-PEG core-shell nanocomposites can rapidly and efficiently convert the 980 nm laser energy into thermal energy, compared with the control experiment of pure water (i.e., 0 ppm) that is only increased by less than 5 °C. Moreover, with the increase of the concentration (i.e., from 3.125 to 6.25, 12.5, 25 and 50 ppm), the temperature of the aqueous dispersion of the nanocomposites can increase by 6.9, 8.7, 10.9, 14.6 and 19.2 °C, respectively, in the same irradiation time of 300 s (Figure 3d). Thus, compared with our previous report on $Cu_9S_5$ nanocrystals,[1c] the $Cu_9S_5$@$mSiO_2$-PEG core-shell nanocomposites not only possess comparable optical absorption characteristic and the photothermal conversion performance, but also are expected to have drug loading and sustained releasing abilities.

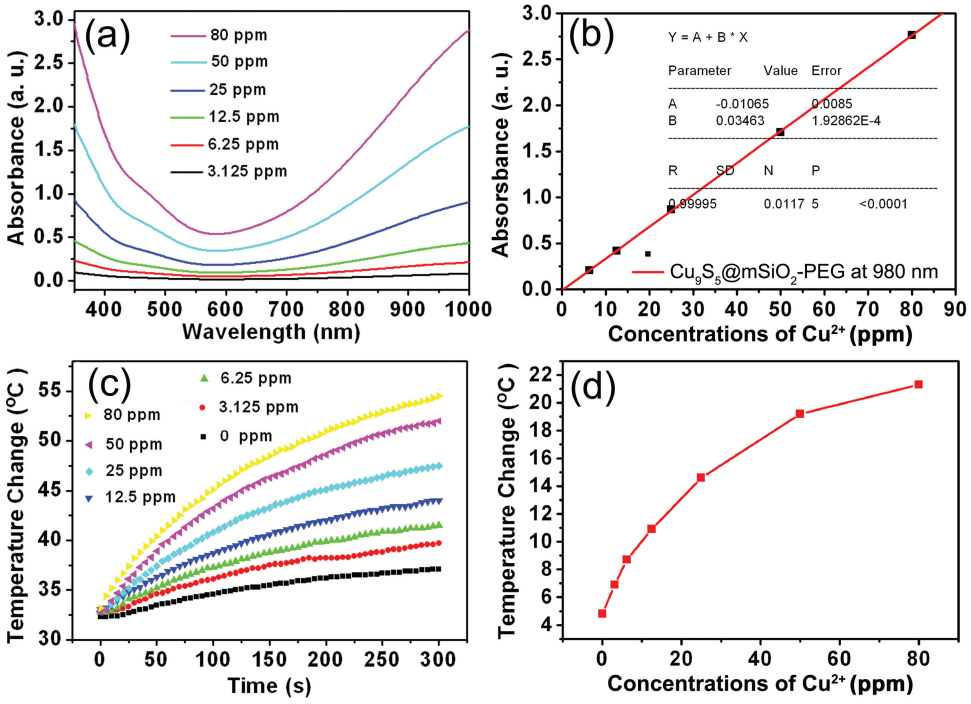


**Figure 3.** a) UV-vis-NIR absorbance spectra for the aqueous solution containing the $Cu_9S_5$@$mSiO_2$-PEG core-shell nanocomposites with a various concentration of $Cu^{2+}$ (i.e., 3.125, 6.25, 12.5, 25, 50 and 80 ppm). b) Plots of linear fitting absorbance versus wavelength at 980 nm for the solutions of the $Cu_9S_5$@$mSiO_2$-PEG core-shell nanocomposites. c) Temperature elevation of the aqueous solution containing the $Cu_9S_5$@$mSiO_2$-PEG nanocomposites with different concentrations of $Cu^{2+}$ (i.e., 3.125, 6.25, 12.5, 25, 50, and 80 ppm) under the irradiation of 980 nm laser with a power density of 0.72 W/cm$^2$ as a function of irradiation time (0–300 s). d) Plot of temperature change over a period of 300 s versus the aqueous dispersion of the $Cu_9S_5$@$mSiO_2$-PEG core-shell nanocomposites (with various concentrations of $Cu^{2+}$).

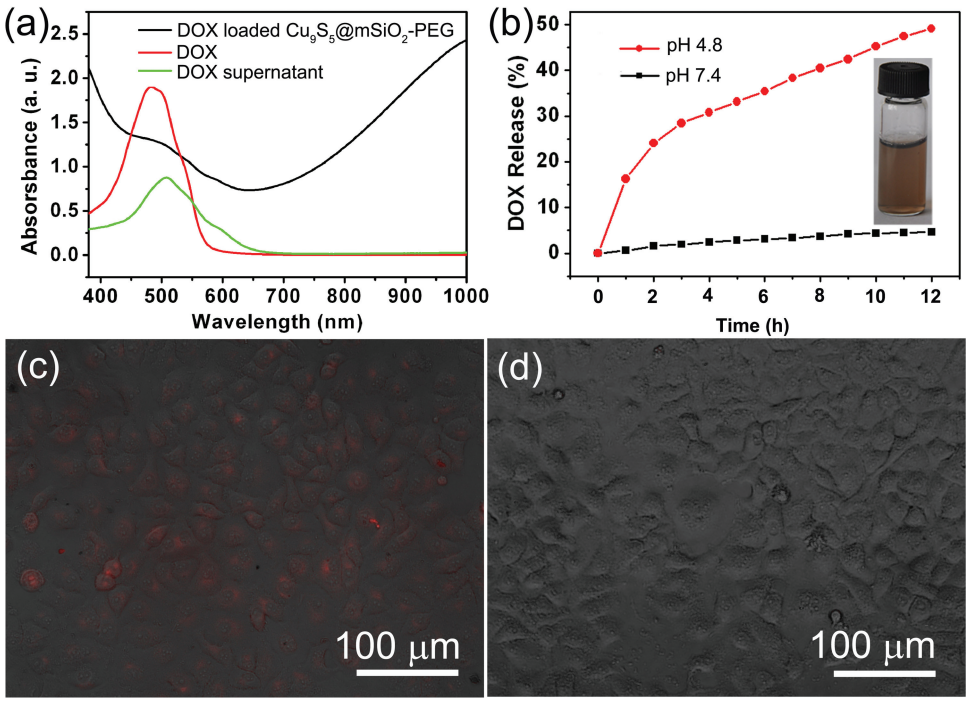


**Figure 4.** a) UV-vis-NIR absorbance spectra of the DOX-loaded $Cu_9S_5$@$mSiO_2$-PEG core-shell nanocomposites, free DOX, and DOX supernatant. The DOX-loaded $Cu_9S_5$@$mSiO_2$-PEG core-shell nanocomposites displayed absorption characteristics of both the DOX and the $Cu_9S_5$@$mSiO_2$-PEG core-shell nanocomposites. b) The cumulative release profile for the complexes of the DOX loaded $Cu_9S_5$@$mSiO_2$-PEG core-shell nanocomposites measured in phosphate-buffer saline (pH 7.4) and acetate buffer (pH 4.8) at room temperature, inset showing a photograph of the complexes of the DOX loaded $Cu_9S_5$@$mSiO_2$-PEG core-shell nanocomposites. c,d) Fluorescence microscopic images of Hep3B cells after 3 h of incubation with the DOX-loaded $Cu_9S_5$@$mSiO_2$-PEG core-shell nanocomposites (c) and free DOX (d), respectively, at the same DOX concentration (8 μg/mL).

Based on our design concept, the mesoporous characteristic of the $Cu_9S_5$@$mSiO_2$-PEG core-shell nanocomposites resulted in a practical use as drug delivery vehicles of loading doxorubicin hydrochloride (DOX, a water-soluble anticancer drug). In our study, the $Cu_9S_5$@$mSiO_2$-PEG core-shell nanocomposites were mixed with DOX for 48 h at room temperature until reaching equilibrium and then repeated washing twice to remove unbound DOX, forming the complexes of the DOX loaded $Cu_9S_5$@$mSiO_2$-PEG core-shell nanocomposites, the aqueous solution of which presents a brown color (**Figure 4**b, inset). The removal of the DOX exhibited a significantly reduced absorbance in UV-Vis region compared with the initial DOX (Figure 4a, green and red curves), while as-formed complexes possessed both the characteristic absorption peak of the DOX and broad plasma absorption band of the $Cu_9S_5$@$mSiO_2$-PEG nanocomposites at the NIR region, which indicates the DOX was successfully incorporated into the $Cu_9S_5$@$mSiO_2$-PEG core-shell nanocomposites (Figure 4a, black curve). An encapsulation efficiency and a loading content of the DOX within the nanocomposites were quantified to be as high as 63.8% and 13.76%, respectively, i.e., per mg of the $Cu_9S_5$@$mSiO_2$-PEG core-shell nanocomposites can load 160 μg of the DOX. Such high loading capability of the present core-shell nanocomposites can be comparable to the reported Au@$mSiO_2$ core-shell nanostructures as drug vehicles (an encapsulation efficiency of 67.8% and a loading content of 14.5%).[4d] In vitro releases of the DOX from the complexes of the DOX loaded $Cu_9S_5$@$mSiO_2$-PEG core-shell nanocomposites were examined in different buffered solutions. Figure 4b shows the cumulative drug release profiles over a period of 12 h in phosphate-buffer saline (PBS, pH 7.4) and acetate buffer (pH 4.8) respectively, at room temperature. At pH 4.8, the cumulative drug release profile (red curve) exhibits a quick release (28% of drug release within 3 h), followed by a sustained, relatively slow release (49% of drug release within 12 h). However, at pH 7.4, a much slower release rate and lower released amount (less than 5% of drug release within 12 h) are observed as a contrast (black curve). Thus, the mesoporous nanostructures of $SiO_2$ shell enable the $Cu_9S_5$@$mSiO_2$-PEG core-shell nanocomposites promising properties of the sustained and pH sensitive drug releases, which could be attributed to the variation of the electrostatic attraction between the mesoporous silica and drug molecules under different pH values.[32] As we know, the DOX is an effective anticancer drug, but adequate dose for cancer treatment usually induces significant side effects. The sustained and pH sensitive release properties of the $Cu_9S_5$@$mSiO_2$-PEG core-shell nanocomposites are favorable for an increased drug accumulation in the cytoplasm of cancer cells following endocytosis and reduced drug release in normal tissue and thus can enhance the long-term chemotherapy efficacy and reduce toxicity.

Moreover, the $Cu_9S_5$@$mSiO_2$-PEG core-shell nanocomposites as a drug carrier can increase drug uptake and accumulation in cancer cells. Since the complexes of the DOX loaded $Cu_9S_5$@$mSiO_2$-PEG core-shell nanocomposites demonstrate negligible fluorescence signals, as compared with a strong

fluorescence emission from the original and free DOX (Supporting Information Figure S6), a fluorescence microscopy was used to observe the drug release inside living cells. Firstly, human hepatocarcinoma cell lines Hep3B were incubated with the DOX loaded $Cu_9S_5$@$mSiO_2$-PEG core-shell nanocomposites (with a DOX concentration of 8 μg/mL) for 3 h and then washed with PBS. As clearly shown in fluorescence microscopy images of Figure 4c, the appearance of intense fluorescence signals from the cells indicates the release of the DOX from the $Cu_9S_5$@$mSiO_2$-PEG core-shell nanocomposites, compared with the weak fluorescence signals with free DOX at the same concentration, shown in Figure 4d, suggesting more DOX could be internalized when it was loaded into the $Cu_9S_5$@$mSiO_2$-PEG nanocomposites. Thus, it can be concluded that as-prepared $Cu_9S_5$@$mSiO_2$-PEG core-shell nanocomposites are beneficial to deliver the DOX into cancer cells.

A high biocompatibility of the $Cu_9S_5$@$mSiO_2$-PEG core-shell nanocomposites is required as a precondition for their applications in cancer treatment. Herein, the influence of the $Cu_9S_5$@$mSiO_2$-PEG nanocomposites on the viabilities of cancer cells and hemolytic behavior of human red blood cells (RBCs) were used to assess the biocompatibility in vitro. Firstly, the $Cu_9S_5$@$mSiO_2$-PEG core-shell nanocomposites with various concentrations (20, 40, 60, 80, 100, 200, 400, 600, 800 and 1000 μg/mL) were incubated with Hep3B cells for 24 h and then the cell viabilities were tested by using the 3-(4,5-dimethylthiazol-2-yl)-2,5-diphenyltetr azolium bromide (MTT) assay. No obviously adverse effect on cells viabilities was observed even the concentration reaching 1000 μg/mL, **Figure 5**a, suggesting a very low cytotoxicity, which excels over the reported 6-amino caproic acid capped $Cu_9S_5$ nanocrystals.[1c] Good blood compatibility is a basis of the successful intravenous administration of the DOX-loaded $Cu_9S_5$@$mSiO_2$-PEG nanocomposites. The effect of the nanocomposites on blood was evaluated by the hemolysis assay of the RBCs, Figure 5b. The hemolytic behavior of the $Cu_9S_5$@$mSiO_2$-PEG nanocomposites was investigated at varying concentrations up to 800 μg/mL, using deionized water and PBS as positive and negative control, respectively, according to the reported protocol.[27] In our experiment, Ethylenediamine tetraacetic acid (EDTA)-stabilized human blood samples were kindly donated by healthy human volunteers. The RBCs were isolated from freshly obtained EDTA-stabilized blood by centrifugation. Then, a ten-fold dilution was performed to yield stable suspensions of the RBCs in PBS. Positive control and negative controls were prepared by mixing as-prepared RBC suspensions with deionized water and PBS, respectively. The concentration of hemoglobin released from the hemolyzed RBCs was determined by measuring the absorbance of the supernatant at 570 nm by UV-vis spectroscopy. It is found that negligible hemolysis of the RBCs can be detected among the $Cu_9S_5$@$mSiO_2$-PEG core-shell nanocomposites with a concentration ranging in 5–800 μg/mL, as shown in Figure 5b. It is suggested that the $Cu_9S_5$@$mSiO_2$-PEG core-shell nanocomposites possess excellent blood compatibility, which is obviously contributed to the pegylated surface of as-prepared nanocomposites.[27] Such excellent blood compatibility is critical to ensure their safety in biomedical applications, and can be comparable to the reported PEG-modified mesoporous silica nanoparticles.[27] Therefore, the negligible cytotoxicity and hemolytic activity demonstrate

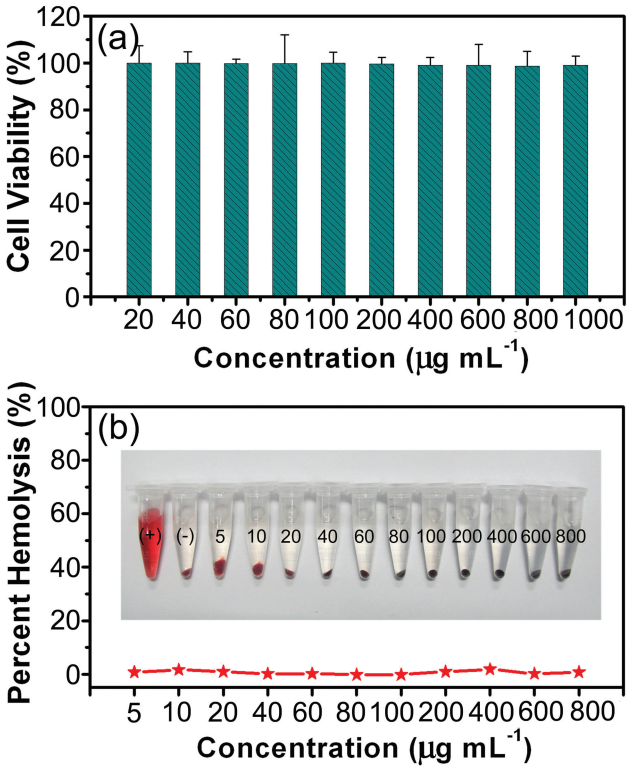


**Figure 5.** a) The viabilities of Hep3B cells incubated with the $Cu_9S_5$@$mSiO_2$-PEG core-shell nanocomposites with different concentrations (20, 40, 60, 80, 100, 200, 400, 600, 800 and 1000 μg/mL) for 24 h, measured by MTT assay. Data represents the mean ± standard deviation of four experiments. b) The hemolytic percent of RBCs incubated with the $Cu_9S_5$@$mSiO_2$-PEG core-shell nanocomposites at various concentrations (5, 10, 20, 40, 60, 80, 100, 200, 400, 600 and 800 μg/mL) for 4 h, using deionized water (+) and PBS (–) as positive and negative controls, respectively, inset showing the photogrpah for direct observation of hemolysis.

that the $Cu_9S_5$@$mSiO_2$-PEG core-shell nanocomposites possess an excellent biocompatibility in vitro and thus can act as a promising platform for cancer treatment.

Since as-synthesized $Cu_9S_5$@$mSiO_2$-PEG core-shell nanocomposites possess effective photothermal conversion characteristic, high drug loading and pH-sensitive release abilities, dual therapeutic modes (DOX release for chemotherapy and hyperthermia) and infrared thermal imagining for cancer treatment are both possible if the tumor cells are irradiated with a laser, as illustrated in **Figure 6**a. The $Cu_9S_5$@$mSiO_2$-PEG core-shell nanocomposites, as a promising photothermal agent, can be a potential as the infrared thermal imaging contrast agent that can monitor the proceeding temperature in real time during the photothermal therapy. To investigate the effect of the $Cu_9S_5$@$mSiO_2$-PEG core-shell nanocomposites as the infrared thermal imaging contrast, two mice with a similar physical appearance were used, in which the left of mouse was injected with 0.15 mL of the $Cu_9S_5$@$mSiO_2$-PEG core-shell nanocomposites (450 μg/mL) via the hypodermic injection to the subcutaneous tissue of back on the marked area (Supporting Information Figure S7b, left), and the other mouse was injected with saline as a control on marked area (Supporting Information

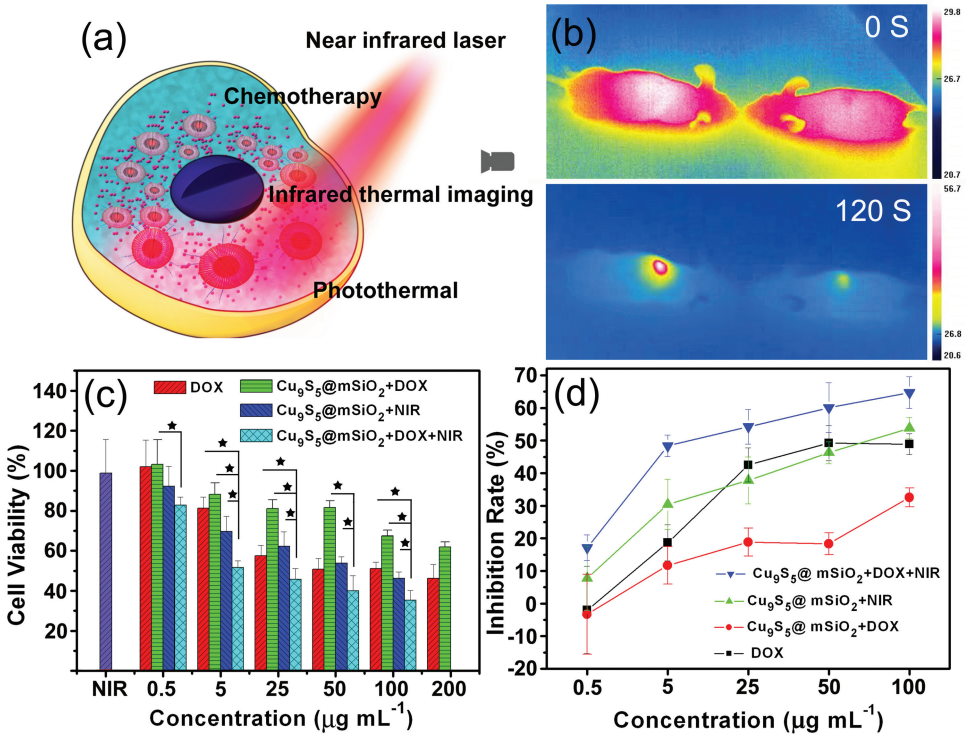


**Figure 6.** a) Schematic illustration of the as-synthesized $Cu_9S_5$@$mSiO_2$-PEG core-shell nanocomposites as a multifunctional nanoplatform for combining photothermal- and chemotherapy with infrared thermal imagining for cancer treatment. b) Infrared thermal imaging of two mice injected with $Cu_9S_5$@$mSiO_2$-PEG core-shell nanocomposites (left mouse, 0.15 mL, 450 μg/mL) or saline (right mouse, the control) via the hypodermic injection, respectively, irradiated with 980 nm laser (0.72 W/cm$^2$) at a time point of 0 and 120 s. The cell viability rate (c) and inhibition rate (d) of the free DOX, the $Cu_9S_5$@$mSiO_2$-PEG core-shell nanocomposites and DOX-loaded $Cu_9S_5$@$mSiO_2$-PEG core-shell nanocomposites incubated with Hep3B cells as a function of the $Cu_9S_5$@$mSiO_2$-PEG concentration. The cells were either exposed to 980 nm laser (0.72 W/cm$^2$) for 3 min or not. Data represents the mean ± standard deviation of four experiments. $P < 0.05$ was considered to be statistically significant difference and shown by asterisks.

Figure S7b, right). Two 980 nm of semiconductor laser devices (an output power density of 0.72 W/cm$^2$) were employed to perpendicularly irradiate the injected areas of two mice, simultaneously. The infrared thermal imaging and temperatures were taken with different time intervals during the laser irradiation, as shown in Figure 6b and Supporting Information Figure S7. Before irradiation, i.e., at 0 s, the whole mice body clearly shows red color, indicating a relatively uniform temperature distribution of two mice. Upon irradiation of the laser, the color dramatically changed. On irradiation for 120 s, the region injected with the $Cu_9S_5$@$mSiO_2$-PEG core-shell nanocomposites shows red color and becomes brighter and larger, while the region injected with saline shows still yellow, compared with the color upon irradiation for 4 s. The injected area of the mouse was heated up very quickly and reached by up to 56.7 from 29.8 °C after 2 min of the irradiation, which was high enough to kill the tumors in vivo. In contrast, less than 5 °C of increase was observed in the control area after 2 min of the irradiation, as shown in Supporting Information Figure S7c. Therefore, it is believable that an infrared thermal imaging function for tumor cells can be obtained by detecting the temperature and color changes induced by the NIR laser irradiation on the $Cu_9S_5$@$mSiO_2$-PEG core-shell nanocomposites.

To investigate the effect of photothermal-, chemotherapy and their combination in vitro, Hep3B cells were incubated with a series of equivalent concentrations of the free DOX, the DOX-loaded $Cu_9S_5$@$mSiO_2$-PEG core-shell nanocomposites, $Cu_9S_5$@$mSiO_2$-PEG core-shell nanocomposites under the NIR laser irradiation, and the DOX-loaded $Cu_9S_5$@$mSiO_2$-PEG core-shell nanocomposites under the NIR laser irradiation (the later three terms are abbreviated hereafter as $Cu_9S_5$@$mSiO_2$ + DOX, $Cu_9S_5$@$mSiO_2$ + NIR, $Cu_9S_5$@$mSiO_2$ + DOX + NIR, respectively). Herein, the $Cu_9S_5$@$mSiO_2$ + DOX and $Cu_9S_5$@$mSiO_2$ + DOX + NIR groups have an equivalent DOX dosage to free DOX group and have an equivalent $Cu_9S_5$@$mSiO_2$ dosage to the $Cu_9S_5$@$mSiO_2$ + NIR group. The cell viabilities (Figure 6c) and the inhibition rates (Figure 6d) as a function of the $Cu_9S_5$@$mSiO_2$-PEG concentration were measured by using the MTT assay. Figure 6c shows that these four groups exhibit the decreased cell viability with increase of concentration and the alone NIR laser irradiation induces no obvious effect on cell viability. The $Cu_9S_5$@$mSiO_2$ + NIR group shows increasing cell inhibition rate with an increase of the concentration (Figure 6d, green curve), demonstrating the $Cu_9S_5$@$mSiO_2$-PEG core-shell nanocomposites can function as the photothermal agent to effectively kill the cancer cells under the irradiation of the NIR laser. Moreover, the DOX released from the DOX-loaded $Cu_9S_5$@$mSiO_2$-PEG core-shell nanocomposites can induce cells' death and the cytotoxicity exhibits in a dose-dependent manner (Figure 6d, red curve). It demonstrates that the $Cu_9S_5$@$mSiO_2$-PEG core-shell nanocomposites can be

further acted as nanocarries of anticancer drug for chemotherapy. More importantly, the $Cu_9S_5$@$mSiO_2$ + DOX + NIR group (Figure 6d, blue curve) shows a significantly enhanced inhibition effect, as compared with that of the free DOX (Figure 6d, black curve), the $Cu_9S_5$@$mSiO_2$-PEG + DOX (Figure 6d, red curve) and Cu9S5@mSiO2 + NIR groups (Figure 6d, green curve) at equivalent concentrations. Notably, at the concentrations of 5, 25, 50 and 100 μg/mL, the P values of the $Cu_9S_5$@$mSiO_2$ + DOX + NIR vs DOX, $Cu_9S_5$@$mSiO_2$ + DOX and $Cu_9S_5$@$mSiO_2$ + NIR groups are all lower than 0.05 except the $Cu_9S_5$@$mSiO_2$ + DOX + NIR vs the DOX group at 50 μg/mL, as shown in Figure 6c, which indicates the statistical significance of differences in the inhibition rate of the $Cu_9S_5$@$mSiO_2$ + DOX + NIR group, as compared with other three groups at these concentrations. Therefore, as-developed $Cu_9S_5$@$mSiO_2$-PEG core-shell nanostructures not only possess the photothermal ablation of cancer cells but also act as drug delivery vehicles for cancer chemotherapy, and importantly the combination of photothermal- and chemotherapy demonstrates better effects on cancer treatment, overmatching individual treatment, in vitro. These results revealed that the DOX loaded $Cu_9S_5$@$mSiO_2$-PEG core-shell nanostructures were a powerful agent for combined chemotherapy and photothermal therapy of cancer in vitro

The as-developed $Cu_9S_5$@$mSiO_2$-PEG core-shell nanocomposites as a phototheraml agent for ablation cancer cell not only function in vitro, but also in vivo. The tumor region was injected with the $Cu_9S_5$@$mSiO_2$-PEG core-shell nanocomposites and then irradiated by 980 nm of laser for 10 min (see detail in Experimental Section and the mice and experimental setup shown in Supporting Information Figure S8). The histological examinations of tumors show degenerative changes of coagulative necrosis, including considerable regions of pyknosis, karyorrhexis, and karyolysis (Supporting Information Figure S9b,d), in comparison with the control sample injected with saline (Supporting Information Figure S9a,c). Therefore, the $Cu_9S_5$@$mSiO_2$-PEG core-shell nanocomposites can also be used as a photothermal agent for effectively destroying the tumor cells in vivo.

To investigate therapeutic efficacy of the DOX-loaded $Cu_9S_5$@$mSiO_2$-PEG core-shell nanocomposites in vivo, comparative studies of inhibiting tumor effectiveness have been conducted. 16 female nude mice of HCT 116 human colon carcinoma model were randomly distributed into four groups, i.e., control group, DOX group, $Cu_9S_5$@$mSiO_2$ + NIR group and $Cu_9S_5$@$mSiO_2$ + DOX + NIR group. Here, the $Cu_9S_5$@$mSiO_2$ + DOX + NIR group has an equivalent DOX dosage to the free DOX group and has an equivalent $Cu_9S_5$@$mSiO_2$-PEG core-shell nanocomposite dosage to the $Cu_9S_5$@$mSiO_2$ + NIR group. Then the tumors of the $Cu_9S_5$@$mSiO_2$ + NIR and $Cu_9S_5$@$mSiO_2$ + DOX + NIR groups were irradiated for 10 min with 980 nm laser (a power density, 0.72 W/cm$^2$). The control group and DOX group received no any irradiation. No mice died during the course of therapy. On the tenth day, mice were sacrificed and tumors were excised and weighed. The tumor photograph and mean tumor weights in each group after the treatment are shown in **Figure 7**a,b. The $Cu_9S_5$@$mSiO_2$ + NIR group showed enhanced inhibition activity than the control

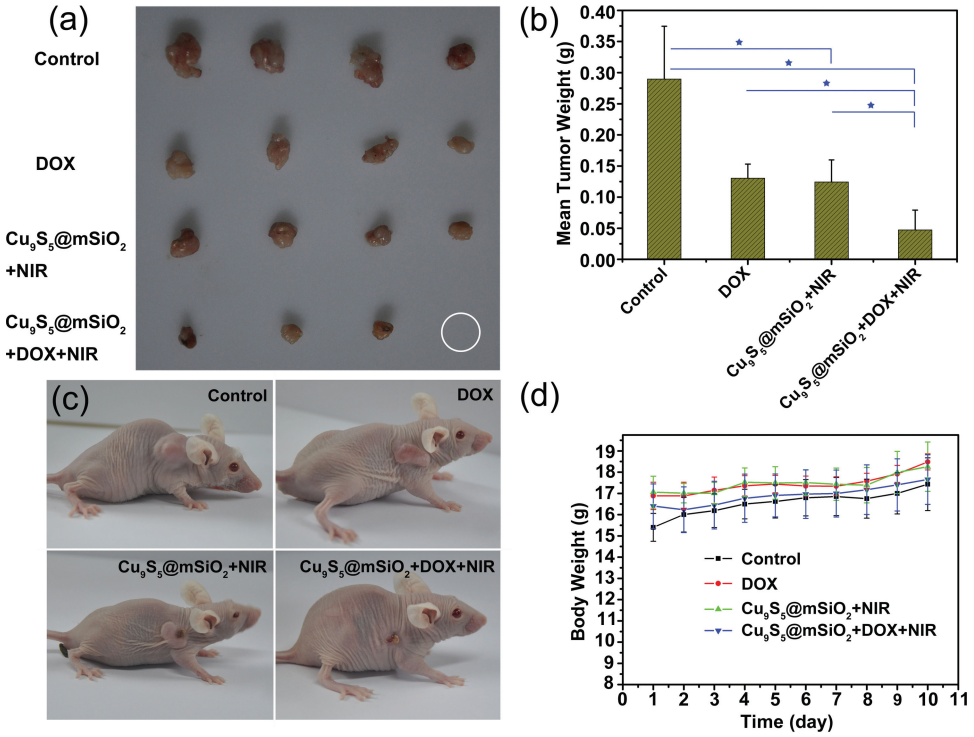


**Figure 7.** a) Photograph of tumors from the control group, DOX group, $Cu_9S_5$@$mSiO_2$ + NIR group and $Cu_9S_5$@$mSiO_2$ + DOX + NIR group, respectively. b) Mean tumor weights after excision from the control group, DOX group, $Cu_9S_5$@$mSiO_2$ + NIR group and $Cu_9S_5$@$mSiO_2$ + DOX + NIR group, respectively. c) Photographs of the test mice on the tenth day. d) Mean body weights of the mice in different groups after treatment. Data represent the mean ± standard deviation of four mice. $P < 0.05$ was considered to be statistically significant difference and shown by asterisks.

group. The mean tumor weight in the $Cu_9S_5$@$mSiO_2$ + NIR group (0.124 ± 0.035 g) was smaller than that of the control group (0.290 ± 0.085 g, $P < 0.05$), which demonstrates that the $Cu_9S_5$@$mSiO_2$-PEG core-shell nanocomposites can effectively inhibit tumor growth in vivo under the NIR laser irradiation. Treatment with the $Cu_9S_5$@$mSiO_2$ + DOX + NIR showed significantly enhanced antitumor activity, as compared with the control group, the free DOX and $Cu_9S_5$@$mSiO_2$ + NIR groups. The mean tumor weight in the $Cu_9S_5$@$mSiO_2$ + DOX + NIR group on day 10 after treatment was 0.047 ± 0.032 g, which was significantly smaller than that of the control group (0.290 ± 0.085 g, $P < 0.05$), DOX group (0.130 ± 0.023 g, $P < 0.05$), and the $Cu_9S_5$@$mSiO_2$ + NIR group (0.124 ± 0.035 g, $P < 0.05$), as shown in Figure 7b.

The region of tumors upon irradiation became whitish immediately after treatment, suggesting disruption of blood perfusion,[33] and further became black scars on the original tumor sites after 1 day treatment. And some of scars were partially fell off after 10 days of post-treatment, as shown in Supporting Information Figure S10. Tumor of the $Cu_9S_5$@$mSiO_2$ + NIR group was not completely inhibited but showed smaller tumor volumes than the control group after treatment, probably due to a small part of the larger size of tumor area free of irradiation.[34] On the other hand, the mice from the $Cu_9S_5$@$mSiO_2$ + DOX + NIR group achieved much smaller tumor weight than the $Cu_9S_5$@$mSiO_2$ + NIR group. The significantly enhanced antitumor activity of the $Cu_9S_5$@$mSiO_2$ + DOX + NIR could probably be attributed to i) a synergistic interaction between chemotherapy and photothermal therapy, both of which were activated simultaneously by 980 nm laser[35] and ii) continuous and slow release of the DOX from the DOX loaded $Cu_9S_5$@$mSiO_2$-PEG core-shell nanocomposites after laser irradiation inhibiting tumor growth for a longtime. Remarkably, one of four mice treated with the $Cu_9S_5$@$mSiO_2$ + DOX + NIR regressed completely and became scar tissue by 10 days of treatment, shown in Figure 7a,c. Thus, the $Cu_9S_5$@$mSiO_2$ + DOX + NIR achieve a significantly enhanced inhibition effect in vivo compared with the $Cu_9S_5$@$mSiO_2$ + NIR and free DOX groups. Besides, considering high toxicity usually leading to a significant weight loss, the body weight of the mice for all groups were measured during the treatments, and no much weight loss was observed (Figure 7d), indicating that the toxicity of treatments was low. Therefore, the as-developed $Cu_9S_5$@$mSiO_2$-PEG core-shell nanocomposites not only possess photothermal treatment ability but also act as drug delivery vehicles for cancer chemotherapy, and importantly the combination of photothermal- and chemotherapy demonstrates better effects on cancer treatment in vivo than individual treatment. These results revealed that the DOX loaded $Cu_9S_5$@$mSiO_2$-PEG core-shell nanocomposites were a powerful agent for combined chemotherapy and photothermal therapy of cancer in vivo. As far as we know, this is the first to realize a combination of photothermal- and chemotherapy based on the $Cu_9S_5$@$mSiO_2$-PEG core-shell nanomaterials. Such a synergistic effect between the photothermal- and chemotherapy of the drug-loaded $Cu_9S_5$@$mSiO_2$-PEG core-shell nanocomposites can endow us a tool to lower the dosage of the DOX by simply using NIR laser irradiation, and thus in this way the toxic side effect induced by high dosage of the drug can be effectively reduced.

## 3. Conclusions

In summary, based on a rational design, the hydrophilic $Cu_9S_5$@$mSiO_2$-PEG core-shell nanocomposites were successfully realized, and not only demonstrated strong NIR region absorption and high photothermal conversion characteristics, but also exhibited excellent biocompatibility in vitro, ensuring their effective photothermal ablation of cancer cells and infrared thermal imaging in vivo. Moreover, due to such a biocompatible mesoporous silica shell, the $Cu_9S_5$@$mSiO_2$-PEG core-shell nanocomposites can serve as a drug carrier for loading DOX for chemotherapy of cancer cells in vitro and in vivo, and importantly showed an enhanced inhibiting rate when combined with photothermal therapy. Although a long-term and systematical toxicity examination in vivo needs many more careful investigations, our results shed light on a promising use of the $Cu_9S_5$@$mSiO_2$-PEG core-shell nanocomposites as a low-toxic and biocompatible multifunctional nanoplateform for a combination of photothermal- and chemotherapy with infrared thermal imagining for tumor cells, and also encourage future research to develop such a multifunctional nanoplateform for cancer diagnosis and therapy with a real potential in the clinic.

## 4. Experimental Section

*Chemicals and Reagents*: All reagents were used without further purification. Anhydrous cupric chloride ($CuCl_2$), sodium diethyldithiocarbamate (SDEDTC), cetyltrimethylammonium bromide (CTAB), sodium hydroxide (NaOH) and anhydrous ethanol are analytically pure and were purchased from Sinopharm Chemical Reagent Co. (Shanghai, China), and tetraethylorthosilicate (TEOS, GR) was obtained from Aladdin and 2-[methoxy(polyethyleneoxy)propyl]-trimethoxysilane (PEG-silane, MW = 596–725 g/mol, 9-12 EO) was obtained from Gelest (Morrisville, PA) and doxorubicin hydrochloride (DOX) was obtained from Huafeng United Technology CO., Ltd. (Beijing, China).

*Characterization*: Powder X-ray diffraction (XRD) was conducted by a D/max-2550 PCX-ray diffractometer (Rigaku, Japan). Sizes, morphologies, and microstructures of the $Cu_9S_5$@$mSiO_2$-PEG core-shell nanocomposites were determined by a transmission electron microscope (TEM; JEM-2100F). The specific surface area and pore volume of the products were determined by Brunauer-Emmett-Teller (BET) and Barett-Joyner-Halenda (BJH) methods (Quantachrome, Autsorb-1MP). UV-Vis-NIR absorption spectra were measured on UV-Vis 1901 Spectrophotometer (Phoenix). Content of copper ions of an aqueous solution containing as-synthesized $Cu_9S_5$ nanocrystals or $Cu_9S_5$@$mSiO_2$-PEG core-shell nanocomposites was determined by a Leeman Laboratories Prodigy high-dispersion inductively coupled plasma atomic emission spectroscopy (ICP-AES). Fourier transform infrared (FTIR) spectra were recorded using the using attenuated total reflectance (ATR) methods on an IRPRESTIGE-21 spectrometer (Shimadzu). Zeta potential measurements were carried out with the Zetasizer Nano Z (Malvern, Britain).

*Synthesis of Copper Diethyldithiocarbamate Precursor*: Copper diethyldithiocarbamate [$Cu(DEDTC)_2$] precursor was prepared by reacting $CuCl_2$ with SDEDTC as follows: SDEDTC (20 mmol) and $CuCl_2$ (10 mmol) were dissolved in distilled water (40 mL) respectively. Then, a solution of SDEDTC was dropwisely added into another solution containing $CuCl_2$ under magnetic stirring, forming a dark brown turbid solution, and then kept for 4 h of continuously stirring. Lastly, the dark brown $Cu(DEDTC)_2$ precursor was obtained by filtration and dried at 60 °C under vacuum for 2 days before use.

*Synthesis of Oleylamine-Capped $Cu_9S_5$ Nanocrystals*: $Cu_9S_5$ nanocrystals were prepared by a modified thermal decomposition method described

previously.[1c] In a typical procedure, 15 mL of oleylamine (OLA) in a flask was degassed at 80 °C in order to remove any moisture and oxygen in which the flask was purged periodically with dry nitrogen gas and subsequently was slowly heated to 300 °C under magnetic stirring for 20 min. Then, another 5 mL of OLA containing 1 mmol of $Cu(DEDTC)_2$ (0.36 g) was injected into the above hot OLA, forming dark green solution immediately, and then was maintained at 300 °C for 10 min before cooling to room temperature. The products were collected via centrifuging at 12000 rpm for 10 min and then were washed and redispersed with hexane and ethanol. Finally, the $Cu_9S_5$ nanocrystals were dispersed in 10 mL of chloroform for later use.

*Synthesis of CTAB-Stabilized $Cu_9S_5$ Nanocrystals ($Cu_9S_5$/CTAB)*: A phase transfer of as-prepared $Cu_9S_5$ nanocrystals from chloroform to water proceeded by a modified method described previously.[14e] First, the above 10 mL of chloroform solution containing the as-prepared $Cu_9S_5$ nanocrystals was mixed with 2 g of CTAB and 80 mL of water. A brown oil-in-water microemulsion appeared and was stirred vigorously at 40 °C for 48 h, and then the chloroform was completely boiled off from the microemulsion under rotary evaporation. As-formed solution was filtered through a 0.22 μm of millipore filter to remove any large aggregates or contaminants and then diluted to 100 mL with distilled water, resulting in a transparent dark green solution of $Cu_9S_5$/CTAB. It is notable that the filtration of process and store of $Cu_9S_5$/CTAB solution should be kept above 25 °C to prevent CTAB precipitation.

*Synthesis of $Cu_9S_5$@m$SiO_2$-PEG Core-Shell Nanocomposites*: Firstly, 3 mL of ethanol was added to the above 50 mL of the $Cu_9S_5$/CTAB solution, followed by ultrasonication and then continuously stirring for 1 h at 60 °C. Then, after addition of 100 μL of NaOH (30 mg/mL) to the solution, 100 μL of TEOS was immediately dropped into this solution under continuously stirring at 60 °C for 1 h, forming a solution containing $Cu_9S_5$@m$SiO_2$ core-shell nanocomposites. Subsequently, 200 μL of PEG-silane was added to as-formed solution upon another 3 h of stirring, resulting in a solution of PEG modified $Cu_9S_5$@m$SiO_2$ core-shell nanocomposites. Finally, the solution was then heated at 90 °C for 6 h in a sealed vessel for hydrothermal treatment in order to enhance the stability of $SiO_2$ shell.[20] The removal of the surfactant proceeded using the method reported previously.[14e,15a,26] The hydrothermal treated sample was washed using ethanol and centrifugated (12000 rpm, 10 min), and then transferred to 50 mL of ethanolic ammonium nitrate (6 mg/mL) upon stirring for 1 h at 60 °C. After that, as-obtained $Cu_9S_5$@m$SiO_2$-PEG core-shell nanocomposites were further washed with ethanol three times. The final products were dispersed into distilled water and stored at 4 °C for later use. For preparation of $Cu_9S_5$@m$SiO_2$ core-shell nanoparticles, all the procedures were similar to that $Cu_9S_5$@m$SiO_2$-PEG core-shell nanocomposites except with no addition of PEG-silane.

*Measurement of Photothermal Performance*: A 980 nm laser was delivered through a quartz cuvette containing aqueous dispersion (0.3 mL) of the $Cu_9S_5$@m$SiO_2$-PEG core-shell nanocomposites with different concentrations of $Cu^{2+}$ (i.e., 0, 3.125, 6.25, 12.5, 25, 50 and 80 ppm). The light source was an external adjustable power (0–0.3 W) 980 nm semiconductor laser device with a 5 mm diameter laser module (Xi'an Tours Radium Hirsh Laser Technology Co., Ltd. China). The output power was independently calibrated using a handy optical power meter (Newport model 1918-C, CA, USA) and was found to be ≈0.3 W for a spot size of ≈0.42 $cm^2$ (i.e., ≈0.72 W/$cm^2$). A thermocouple with an accuracy of 0.1 °C was inserted into the aqueous dispersion of the $Cu_9S_5$@m$SiO_2$-PEG core-shell nanocomposites, which was oriented perpendicular to the path of the laser beam. The temperature was recorded one time per 5 s.

*Drug Loading and In Vitro Release*: 12 mg of as-synthesized $Cu_9S_5$@m$SiO_2$-PEG core-shell nanocomposites and 30 mL of DOX (0.1 mg/mL) solution were mixed and stirred at room temperature for 48 h to reach the equilibrium state. The DOX-loaded $Cu_9S_5$@m$SiO_2$-PEG core-shell nanocomposites ($Cu_9S_5$@m$SiO_2$-PEG + DOX) were collected by centrifugation at 12000 rpm for 10 min and washed two times with water to remove the unbound DOX and then a supernatant solution was collected. The amount of loaded DOX into the $Cu_9S_5$@m$SiO_2$-PEG core-shell nanocomposites was determined by a UV-Vis spectrophotometer at 482.4 nm. An entrapment efficiency and a loading content of the DOX within the nanocomposites were calculated by the following equations: encapsulation efficiency = weight of DOX in the $Cu_9S_5$@m$SiO_2$-PEG/initial weight of DOX, loading content = weight of DOX in the $Cu_9S_5$@m$SiO_2$-PEG/weight of the $Cu_9S_5$@m$SiO_2$-PEG + DOX. In the drug release experiment in vitro, as-prepared $Cu_9S_5$@m$SiO_2$-PEG + DOX complexes were dispersed in 5 mL of PBS (pH 7.4) and 5 mL of acetate buffer (pH 4.8), respectively, by stirring and ultrasonication, forming two solutions of 1 mg/mL, i.e., release mediums. Both of the release mediums were agitated at room temperature and then were centrifuged at an interval of 1 h. 4 mL of each supernatant solution was collected and the same volumes of fresh buffers were added to the residual dispersion of the $Cu_9S_5$@m$SiO_2$-PEG + DOX complexes. The amounts of the released DOX in the supernatant solutions were measured by a UV-Vis spectrometer at 482.4 nm.

*Hemolysis Assay*: Ethylenediamine tetraacetic acid (EDTA)-stabilized human blood samples were kindly donated by healthy human volunteers. First, 5 mL of blood sample was added to 10 mL of PBS, and then red blood cells (RBCs) were isolated from serum by centrifugation at 3000 rpm/min for 10 min. The RBCs were further washed five times with 10 mL of PBS solution, and then diluted into 50 mL of PBS. Herein, the RBC incubation with distilled water and PBS were used as the positive and negative controls, respectively. 0.2 mL of diluted RBC suspension was added to 0.8 mL of PBS solution containing the $Cu_9S_5$@m$SiO_2$-PEG core-shell nanocomposites with different concentrations. All the samples were kept for 4 h in static condition at room temperature. Finally, the samples were centrifuged at 12000 rpm/min for 10 min, and 100 μL of supernatant solution was obtained from each sample, respectively, for measuring the absorbance values at 570 nm. The percent hemolysis of the RBCs was calculated using the following formula: percent hemolysis = ((sample absorbance - negative control absorbance)/(positive control absorbance- negative control absorbance)) × 100%.

*Cell Culture*: Human hepatocarcinoma cell lines Hep3B were maintained in Dulbecco's modified Eagle's medium (high glucose) (GIBCO, Invitrogen) and supplemented with 10% fetal bovine serum, 100 units/mL penicillin, and 100 mg/mL streptomycin in a humidified incubator under 5% $CO_2$ at 37 °C.

*Fluorescence Imaging*: Hep3B cells were seeded in a 24-well plate and cultured for 24 h. The cell medium was removed, and then cells were incubated with 0.3 mL of culture medium containing the DOX-loaded $Cu_9S_5$@m$SiO_2$-PEG core-shell nanocomposites and free DOX, respectively, at the same DOX concentration (8 μg/mL) for another 3 h. Cell imaging was then carried out after washing cells with PBS.

*In Vitro Cytotoxicity of the $Cu_9S_5$@m$SiO_2$-PEG Core-Shell Nanocomposites*: Hep3B cells were seeded in a 96-well plate at a density of $1 \times 10^4$ cells/well for 24 h at 37 °C in 5% $CO_2$ to allow the cells to attach. The culture medium was changed and cells were incubated with complete medium containing the $Cu_9S_5$@m$SiO_2$-PEG core-shell nanocomposites at a series of concentrations (20, 40, 60, 80, 100, 200, 400, 600, 800 and 1000 μg/mL) at 37 °C with 5% $CO_2$ for further 24 h. After that, 0.1 mL of 3-(4, 5)-dimethylthiahiazo-2-yl)-2,5-diphenyltetrazolium bromide (MTT) solution (5 mg/mL, Sigma, Cat. M2003) was added to each well of the microtiter plate and then was incubated in the $CO_2$ incubator for 4 h. The cells then were lysed by the addition of 100 μL of DMSO. The spectrophotometric absorbance of formazan was measured using a plate reader at 490 nm. Four replicates were done for each treatment group.

*In Vitro Inhibition Rate of Free DOX and the $Cu_9S_5$@m$SiO_2$-PEG and $Cu_9S_5$@m$SiO_2$-PEG + DOX Nanocomposites*: Hep3B cells were seeded in a 96-well plate at a density $1 \times 10^4$ cells/well for 24 h at 37 °C in 5% $CO_2$ to allow the cells to attach. The culture medium was changed and cells were incubated with complete medium containing DOX, the $Cu_9S_5$@m$SiO_2$-PEG and $Cu_9S_5$@m$SiO_2$-PEG + DOX at an equivalent concentration. After 4 h of incubation, excess unbound nanocomposites were removed by rinsing three times with PBS. Fresh complete medium was then added to the wells. The cells were exposed to 980 nm laser at an output power density of 0.72 W/$cm^2$ for 3 min for photothermal

and photothermal-chemotherapy treatments, respectively, and then incubated again at 37 °C with 5% $CO_2$ for further 24 h. After this treatment, MTT assay was tested to evaluate the cell viabilities. Four replicates were done for each treatment group.

*In Vivo Infrared Thermal Imaging*: Infrared thermal imaging in vivo was performed with a photothermal therapy-monitoring system GX-A300 (Shanghai Guixin Corporation). Two mice were first anaesthetized by trichloroacetaldehyde hydrate (10%) at a dosage of 40 mg/kg body weight, and then injected with 0.15 mL of PBS buffer solution containing the $Cu_9S_5$@m$SiO_2$-PEG (450 μg/mL) core-shell nanocomposites and saline as a control, respectively, via the hypodermic injection to the subcutaneous tissue of back. Two 980 nm of semiconductor laser devices (Xi'an Tours Radium Hirsh Laser Technology Co., Ltd. China) were independently calibrated to be the same output power density of 0.72 W/cm$^2$ using a handy optical power meter (Newport model 1918-C, CA, USA), which were oriented perpendicular to the injected areas of two mice, respectively. The two mice were then irradiated within 5 min after injection to prevent nanocomposites diffusing completely. The temperature of irradiated area was recorded one time per 5 second. All the experiments were carried out at room temperature of 20 °C.

*In Vivo Photothermal Ablation of Cancer Cells*: Severe combined immunodeficiency mice (SCID) were inoculated subcutaneously with $4 \times 10^6$ hepatocarcinoma cell lines Hep3B cells on the left side of the rear leg 4–5 weeks before the experiment. When tumors grew to 7–12 mm in diameter, the SCID mice were labeled as control and treatment samples. Two nude mice were first anaesthetized by trichloroacetaldehyde hydrate (10%) at a dosage of 40 mg/kg body weight, and then the treatment and control samples were injected with 0.15 mL of PBS solution containing the $Cu_9S_5$@m$SiO_2$-PEG core-shell nanocomposites (450 μg/mL) and saline, respectively, at the central region of the tumors with a depth of ~4 mm. After 1 h, the tumors on the control and treatment were irradiated with 980 nm laser (an output power density of 0.72 W/cm$^2$) for 10 min. After that, the two SCID mice were scarified and tumors were removed, embedded in paraffin, and cryosectioned into 4 μm slices. These slides were stained with hematoxylin/eosin, and examined under a Zeiss Axiovert 40 CFL inverted fluorescence microscope, and images were captured with a Zeiss AxioCam MRc5 digital camera.

*In Vivo Antitumor Effect*: HCT 116 human colon carcinoma cells were cultured in McCoy's 5A (Hyclone) supplemented with 10% v/v heat-inactivated fetal bovine serum (Biochrom), 2 mM L-glutamine (Gibco), penicillin (100 U/mL) (Sigma), and streptomycin (100 μg/mL) (Gibco in a 5% $CO_2$ humidified atmosphere. Female BALB/c nude mice, 4-5 weeks of age, were obtained from BK (Shanghai). Tumors were generated by subcutaneous injection of HCT 116 cells (about $5.0 \times 10^6$cells/mouse). When the mean tumor reached approximately 3 mm in diameter, the mice were divided into four groups with each of four mice, minimizing the differences of weights and tumor sizes in each group. The mice were administered with a) PBS (200 μL), b) DOX (200 μL, 0.4 mg/kg), c) $Cu_9S_5$@m$SiO_2$-PEG (200 μL, 2.5 mg/kg, in terms of $Cu_9S_5$@m$SiO_2$-PEG), and d) DOX loaded-$Cu_9S_5$@m$SiO_2$-PEG (200 μL, 2.5 mg/kg, in terms of $Cu_9S_5$@m$SiO_2$-PEG), through intratumor injection. Then, the tumor regions of the $Cu_9S_5$@m$SiO_2$-PEG group and DOX loaded-$Cu_9S_5$@m$SiO_2$-PEG group were irradiated with 980 nm laser (a power density of 0.72 W/cm$^2$, an irradiation time of 10 min) through the skin surface within 5 min after injection to limit nanoparticle diffusion beyond the tumor boundaries. After the experiments were finished, mice were killed by $CO_2$ asphyxiation and the tumors were collected and weighed. All animals were handled following the protocols reviewed and approved by the Institutional Animal Care and Use Committee (IACUC).

*Statistical Analysis:* Data are expressed as mean ± standard deviation. Student's t-test was used for statistical analyses.

## Supporting Information

Supporting Information is available from the Wiley Online Library or from the author.

## Acknowledgements

G.S., Q.W., Y.W., and G.L. contributed equally to this work. This work was financially supported by the National Natural Science Foundation of China (Grant No. 21171035 and 51272299), the Key Grant Project of Chinese Ministry of Education (Grant No. 313015), the Scientific Research Foundation for the Returned Overseas Chinese Scholars, the Science and Technology Commission of Shanghai-based "Innovation Action Plan" Project (Grant No. 10JC1400100), Shanghai Rising-Star Program (Grant No. 11QA1400100), Innovation Program of Shanghai Municipal Education Commission (Grant No. 13ZZ053), Ph.D. Programs Foundation of Ministry of Education of China (Grant No. 20110075110008), the Fundamental Research Funds for the Central Universities, Shanghai Leading Academic Discipline Project (Grant No. B603), and the Program of Introducing Talents of Discipline to Universities (Grant No. 111-2-04).

Received: November 12, 2012
Revised: February 5, 2013
Published online: April 9, 2013

[1] a) S. Lal, S. E. Clare, N. J. Halas, *Acc. Chem. Res.* **2008**, *41*, 1842–1851; b) L. Cheng, K. Yang, Q. Chen, Z. Liu, *ACS Nano* **2012**, *6*, 5605–5613; c) Q. Tian, F. Jiang, R. Zou, Q. Liu, Z. Chen, M. Zhu, S. Yang, J. Wang, J. Wang, J. Hu, *ACS Nano* **2011**, *5*, 9761–9771.

[2] a) E. I. Altinoglu, J. H. Adair, *Wiley Interdiscip. Rev. Nanomed. Nanobiotechnol.* **2010**, *2*, 461–477; b) Q. Tian, M. Tang, Y. Sun, R. Zou, Z. Chen, M. Zhu, S. Yang, J. Wang, J. Wang, J. Hu, *Adv. Mater.* **2011**, *23*, 3542–3547.

[3] a) E. Boisselier, D. Astruc, *Chem. Soc. Rev.* **2009**, *38*, 1759–1782; b) X. H. Huang, P. K. Jain, I. H. El-Sayed, M. A. El-Sayed, *Nanomedicine* **2007**, *2*, 681–693; c) J. Geng, K. Li, K.-Y. Pu, D. Ding, B. Liu, *Small* **2012**, *8*, 2421–2429.

[4] a) E. B. Dickerson, E. C. Dreaden, X. H. Huang, I. H. El-Sayed, H. H. Chu, S. Pushpanketh, J. F. McDonald, M. A. El-Sayed, *Cancer Lett.* **2008**, *269*, 57–66; b) B. Jang, J. Y. Park, C. H. Tung, I. H. Kim, Y. Choi, *ACS Nano* **2011**, *5*, 1086–1094; c) C. G. Wang, J. Chen, T. Talavage, J. Irudayaraj, *Angew. Chem. Int. Ed.* **2009**, *48*, 2759–2763; d) Z. Zhang, L. Wang, J. Wang, X. Jiang, X. Li, Z. Hu, Y. Ji, X. Wu, C. Chen, *Adv. Mater.* **2012**, *24*, 1418–1423.

[5] Y. Xia, W. Li, C. M. Cobley, J. Chen, X. Xia, Q. Zhang, M. Yang, E. C. Cho, P. K. Brown, *Acc. Chem. Res.* **2011**, *44*, 914–924.

[6] a) H. Liu, T. Liu, X. Wu, L. Li, L. Tan, D. Chen, F. Tang, *Adv. Mater.* **2012**, *24*, 755–761; b) H. Liu, D. Chen, L. Li, T. Liu, L. Tan, X. Wu, F. Tang, *Angew. Chem. Int. Ed.* **2011**, *50*, 891–895.

[7] X. Q. Huang, S. H. Tang, X. L. Mu, Y. Dai, G. X. Chen, Z. Y. Zhou, F. X. Ruan, Z. L. Yang, N. F. Zheng, *Nat. Nanotechnol.* **2011**, *6*, 28–32.

[8] a) X. Wang, C. Wang, L. Cheng, S.-T. Lee, Z. Liu, *J. Am. Chem. Soc.* **2012**, *134*, 7414–7422; b) V. S. Thakare, M. Das, A. K. Jain, S. Patil, S. Jain, *Nanomedicine* **2010**, *5*, 1277–1301.

[9] a) M. Li, X. Yang, J. Ren, K. Qu, X. Qu, *Adv. Mater.* **2012**, *24*, 1722–1728; b) J. T. Robinson, S. M. Tabakman, Y. Liang, H. Wang, H. S. Casalongue, V. Daniel, H. Dai, *J. Am. Chem. Soc.* **2011**, *133*, 6825–6831; c) S.-H. Hu, Y.-W. Chen, W.-T. Hung, I. W. Chen, S.-Y. Chen, *Adv. Mater.* **2012**, *24*, 1748–1754; d) K. Yang, L. Hu, X. Ma, S. Ye, L. Cheng, X. Shi, C. Li, Y. Li, Z. Liu, *Adv. Mater.* **2012**, *24*, 1868–1872.

[10] K. Yang, H. Xu, L. Cheng, C. Sun, J. Wang, Z. Liu, *Adv. Mater.* **2012**, *24*, 5586–5592.

[11] J. Yang, J. Choi, D. Bang, E. Kim, E. K. Lim, H. Park, J. S. Suh, K. Lee, K. H. Yoo, E. K. Kim, Y. M. Huh, S. Haam, *Angew. Chem. Int. Ed.* **2011**, *50*, 441–444.

[12] a) M. Zhou, R. Zhang, M. A. Huang, W. Lu, S. L. Song, M. P. Melancon, M. Tian, D. Liang, C. Li, *J. Am. Chem. Soc.* **2010**,

*132*, 15351–15358; b) C. M. Hessel, V. P. Pattani, M. Rasch, M. G. Panthani, B. Koo, J. W. Tunnell, B. A. Korgel, *Nano Lett.* **2011**, *11*, 2560–2566; c) Y. B. Li, W. Lu, Q. A. Huang, M. A. Huang, C. Li, W. Chen, *Nanomedicine* **2010**, *5*, 1161–1171.

[13] T. L. Doane, C. Burda, *Chem. Soc. Rev.* **2012**, *41*, 2885–2911.

[14] a) T. T. Tan, S. T. Selvan, L. Zhao, S. Gao, J. Y. Ying, *Chem. Mater.* **2007**, *19*, 3112–3117; b) Z. Zhelev, H. Ohba, R. Bakalova, *J. Am. Chem. Soc.* **2006**, *128*, 6324–6325; c) Y. Yang, L. Jing, X. Yu, D. Yan, M. Gao, *Chem. Mater.* **2007**, *19*, 4123–4128; d) C. W. Lai, Y. H. Wang, Y. C. Chen, C. C. Hsieh, B. P. Uttam, J. K. Hsiao, C. C. Hsua, P. T. Chou, *J. Mater. Chem.* **2009**, *19*, 8314–8319; e) Y.-K. Peng, C.-W. Lai, C.-L. Liu, H.-C. Chen, Y.-H. Hsiao, W.-L. Liu, K.-C. Tang, Y. Chi, J.-K. Hsiao, K.-E. Lim, H.-E. Liao, J.-J. Shyue, P.-T. Chou, *ACS Nano* **2011**, *5*, 4177–4187.

[15] a) W. Fang, J. Yang, J. Gong, N. Zheng, *Adv. Funct. Mater.* **2012**, *22*, 842–848; b) Y. Zhao, L.-N. Lin, Y. Lu, S.-F. Chen, L. Dong, S.-H. Yu, *Adv. Mater.* **2010**, *22*, 5255–5259.

[16] a) C. E. Ashley, E. C. Carnes, K. E. Epler, D. P. Padilla, G. K. Phillips, R. E. Castillo, D. C. Wilkinson, B. S. Wilkinson, C. A. Burgard, R. M. Kalinich, J. L. Townson, B. Chackerian, C. L. Willman, D. S. Peabody, W. Wharton, C. J. Brinker, *ACS Nano* **2012**, *6*, 2174–2188; b) M.-H. Kim, H.-K. Na, Y.-K. Kim, S.-R. Ryoo, H. S. Cho, K. E. Lee, H. Jeon, R. Ryoo, D.-H. Min, *ACS Nano* **2011**, *5*, 3568–3576.

[17] H. Wu, G. Liu, S. Zhang, J. Shi, L. Zhang, Y. Chen, F. Chen, H. Chena, *J. Mater. Chem.* **2011**, *21*, 3037–3045.

[18] L. Pan, Q. He, J. Liu, Y. Chen, M. Ma, L. Zhang, J. Shi, *J. Am. Chem. Soc.* **2012**, *134*, 5722–5725.

[19] a) X. Yang, X. Liu, Z. Liu, F. Pu, J. Ren, X. Qu, *Adv. Mater.* **2012**, *24*, 2890–2895; b) Y.-T. Chang, P.-Y. Liao, H.-S. Sheu, Y.-J. Tseng, F.-Y. Cheng, C.-S. Yeh, *Adv. Mater.* **2012**, *24*, 3309–3314.

[20] Y.-S. Lin, N. Abadeer, C. L. Haynes, *Chem. Commun.* **2011**, *47*, 532–534.

[21] C.-W. Lai, Y.-H. Wang, C.-H. Lai, M.-J. Yang, C.-Y. Chen, P.-T. Chou, C.-S. Chan, Y. Chi, Y.-C. Chen, J.-K. Hsiao, *Small* **2008**, *4*, 218–224.

[22] H. X. Wu, S. J. Zhang, J. M. Zhang, G. Liu, J. L. Shi, L. X. Zhang, X. Z. Cui, M. L. Ruan, Q. J. He, W. B. Bu, *Adv. Funct. Mater.* **2011**, *21*, 1850–1862.

[23] I. Gorelikov, N. Matsuura, *Nano Lett.* **2008**, *8*, 369–373.

[24] R. I. Nooney, D. Thirunavukkarasu, Y. M. Chen, R. Josephs, A. E. Ostafin, *Langmuir* **2003**, *19*, 7628–7637.

[25] N. Lewinski, V. Colvin, R. Drezek, *Small* **2008**, *4*, 26–49.

[26] Y.-S. Lin, N. Abadeer, K. R. Hurley, C. L. Haynes, *J. Am. Chem. Soc.* **2011**, *133*, 20444–20457.

[27] Y.-S. Lin, C. L. Haynes, *J. Am. Chem. Soc.* **2010**, *132*, 4834–4842.

[28] H. Wang, M. Peng, J. Zheng, P. Li, *J. Colloid Interface Sci* **2008**, *326*, 151–157.

[29] N. Moussaif, S. Irusta, C. Yagüe, M. Arruebo, J. G. Meier, C. Crespo, M. A. Jimenez, J. Santamaría, *Polymer* **2010**, *51*, 6132–6139.

[30] V. Cauda, C. Argyo, T. Bein, *J. Mater. Chem.* **2010**, *20*, 8693–8699.

[31] J. M. Luther, P. K. Jain, T. Ewers, A. P. Alivisatos, *Nat. Mater.* **2011**, *10*, 361–366.

[32] a) J. Vora, N. Bapat, M. Boroujerdi, *Drug Dev. Ind. Pharm.* **1993**, *19*, 759–771; b) G. Song, C. Li, J. Hu, R. Zou, K. Xu, L. Han, Q. Wang, J. Yang, Z. Chen, Z. Qin, K. Ruan, R. Hu, *J. Mater. Chem.* **2012**, *22*, 17011–17018.

[33] J. You, R. Zhang, C. Xiong, M. Zhong, M. Melancon, S. Gupta, A. M. Nick, A. K. Sood, C. Li, *Cancer Res.* **2012**, *72*, 4777–4786.

[34] W. Zhang, Z. Guo, D. Huang, Z. Liu, X. Guo, H. Zhong, *Biomaterials* **2011**, *32*, 8555–8561.

[35] J. You, R. Zhang, G. Zhang, M. Zhong, Y. Liu, C. S. Van Pelt, D. Liang, W. Wei, A. K. Sood, C. Li, *J. Controlled Release* **2012**, *158*, 319–328.